Aeroelastic control of a smart composite plate with delaminations

Changho Nam, Aditi Chattopadhyay, Youdan Kim

Changho Nam, Aditi Chattopadhyay, Youdan Kim, "Aeroelastic control of a smart composite plate with delaminations," Proc. SPIE 3668, Smart Structures and Materials 1999: Smart Structures and Integrated Systems, (9 June 1999); doi: 10.1117/12.350694

SPIE.

Event: 1999 Symposium on Smart Structures and Materials, 1999, Newport Beach, CA, United States

Aeroelastic Control of Smart Composite Plate with Delaminations

Changho Nam*[a], Aditi Chattopadhyay[a], Youdan Kim[b]

[a]Dept. of Mechanical and Aerospace Eng., Arizona State University, Tempe, AZ 85287-6106
[b]Dept. of Aerospace Eng., Seoul National University, Seoul, South Korea

ABSTRACT

In this paper, aeroelastic performance of smart composite wing in the presence of delaminations is investigated. A control system is designed to enhance the dynamic stability of the delaminated composite wing. The refined higher order theory for analyzing an adaptive composite plate in the presence of delaminations is used. The theory accurately captures the transverse shear deformation through the thickness, which is important in anisotropic composites, particularly in the presence of discrete actuators and sensors and delaminations. The effects of delamination on the aeroelastic characteristics of composite plates are investigated. An active control system is designed to redistribute the loads and to minimize the effect of delamination. The pole placement technique is applied to design the closed loop system by utilizing piezoelectric actuators. Due to delamination, the significant changes in the natural frequencies of the lower modes are observed. And this causes the reduction on the flutter speed of the delaminated plate model. The aeroelastic control results show that controller makes the delaminated plate model behave like a normal plate. The controller also reduces a significant amount of RMS values of the gust response due to gust.

Keywords: smart structures, delaminations, aeroelastic control, piezoelectric actuators

1. INTRODUCTION

Research and development of smart materials and smart structural systems has been actively pursued in the last decade. Recently, smart composite structures have received considerable attention due to the great potential for static and dynamic control [1-3]. In designing with smart composites, it is important to take into consideration imperfections, such as delaminations, that may be pre-existing or may develop during the service lift of the structure. Delaminations will have significant impact on piezoelectric actuator performance and vibration characteristics of the structure, such as changes in mode shapes and frequencies. A significant amount of research has also been performed in modeling defects such as delamination in composites. Although three dimensional approaches [4,5] are more accurate than two dimensional theories [6-9], their implementation can be very expensive for practical applications. The layer-wise approach [10] is an alternative since it is capable of modeling displacement discontinuities. However, the computational effort increases with the number of plies. Recently, a refined higher order theory, developed by Chattopadhyay and Gu [11], was shown to be both accurate and efficient for modeling delamination in composite plates and shells of moderately thick construction. This theory has also been shown to agree well with both elasticity solutions [12] and experimental results [11,13]. Relatively little attention has been paid to detailed modeling issues associated with adaptive composite structures with surface bonded/embedded piezoelectric actuators and sensors including debonding [13-16]. In most of the existing work, the actuators are assumed to be perfectly embedded or bonded to the primary structure. However, it has recently been shown by Seeley and Chattopadhyay [17] that the control authority of smart structures can be significantly mispredicted in the presence of debonding.

The effects of delamination in reducing structural integrity and altering the dynamic characteristics of the structure have been well established. However, their influence on the aeroelastic performance of composite wing sections has not been investigated. The objective of this paer is to investigate in aeroelastic performance of smart composite wing in the presence

*On leave from Hankuk Aviation University, Koyang, South Korea, Correspondence:Email: chnam@imap4.asu.edu; Telephone: 602-965-5864; Fax: 602-965-1384

Part of the SPIE Conference on Smart Structures and Integrated Systems
Newport Beach, California • March 1999
SPIE Vol. 3668 • 0277-786X/99/$10.00

of delaminations. A control system is also designed to enhance the dynamic stability of the delaminated composite wing. For the structural analysis of the delaminated smart composite wing, a higher order refined theory developed by Seeley and Chattopadhyay is used [18]. In this theory, the smart composite structure is divided into regions representing the nondelaminated zone and portions of the composite laminate above and below the delamination. The refined theory is implemented in each region and the stress free boundary conditions are imposed at the top and bottom surfaces of the laminate as well as at the delamination interfaces. This allows several of the higher order functions to be identified in terms of the lower order functions. Continuity conditions are also formulated between the regions. These conditions are enforced in the finite element implementation using a penalty approach. A doublet lattice method is used to compute the unsteady aerodynamic forces and the unsteady gust forces. The aerodynamic forces are approximated as the transfer functions of the Laplace variable using a least square curve fit approximation to define the aeroservoelastic equations of motion in a linear time invariant state-space form. The aeroelastic characteristics of the open loop system for a composite wing with delaminations are investigated. To design the control system, pole placement technique with output feedback is used in this study. The eigenvalues of the elastic modes are assigned to the desired values using a pole placement technique. For a given configuration, that is, with specified locations of the actuators, the effect of delamination on each piezoelectric actuator is investigated.

2. MATHEMATICAL FORMULATION

2.1. Finite Element Modeling of Delaminated Composite Plate

The geometry of the smart composite laminate, including delamination, is shown in Fig. 1. The general displacement field, based on the higher order theory, is defined as follows [18].

$$\begin{aligned} U(x,y,z) &= u(x,y)+(z-c)\left(-\frac{\partial}{\partial x}w(x,y)+\phi_x(x,y)\right)+(z-c)^2u_2(x,y)+(z-c)^3u_3(x,y) \\ V(x,y,z) &= v(x,y)+(z-c)\left(-\frac{\partial}{\partial y}w(x,y)+\phi_y(x,y)\right)+(z-c)^2v_2(x,y)+(z-c)^3v_3(x,y) \\ W(x,y,z) &= w(x,y) \end{aligned} \tag{1}$$

where U, V and W are the total displacements and u, v and w denote the midplane displacements of a point (x,y). The partial derivatives of w represent the rotations of normals to the midplane corresponding to the slope of the laminate and ϕ_x and ϕ_y represent the additional rotations due to shear deformation about the y and x axes, respectively. The quantities u_2, u_3, v_2 and v_3 represent higher order functions. This displacement field has the advantage of easily reducing to the well known classical theory if the higher order terms are eliminated. The thickness coordinate, z, is measured from the global midplane of the laminate. Note that c = 0 in the region representing the nondelaminated portion of the composite.

The expressions relating the stress, strain, charge and electric field are derived from the electric enthalpy density function [18]. For an orthotropic composite laminate with piezoelectric layers, the constitutive relationships are simplified as follows.

$$\{\sigma\} = [\overline{Q}]\{\varepsilon - \Lambda\} \tag{2}$$

where Λ are the induced strains ($\Lambda_1 = \Lambda_2 = d_{31}E_3$).

To account for the effects due to delamination, it is necessary to partition the laminate into several different regions. These regions include the delaminated region, the region above the delamination and the region below the delamination. The general form of the higher order displacement field (Eqn. 1) is independently applied to each of these regions to describe displacements which account for slipping and separation due to the delamination. However, this displacement field does not necessarily satisfy the condition that the transverse shear stresses (σ_4 and σ_5), vanish at the top and bottom surfaces of the plate ($z = \pm h/2$) as well as on the delamination interface surfaces ($z = h_1$, Fig. 1) in the delaminated region. That is,

$$\sigma_4(x,y,\pm h/2)=0,\quad \sigma_5(x,y,\pm h/2)=0 \qquad (x,y)\in\Omega^r(r=u,d1,d2) \tag{3}$$

$$\sigma_4(x,y,h_1)=0,\quad \sigma_5(x,y,h_1)=0 \qquad (x,y)\in\Omega^r(r=d1,d2) \tag{4}$$

in which the superscript r corresponds to either the nondelaminated region (u), or the regions above and below the delamination (d1 and d2), respectively. For orthotropic plates, these conditions are equivalent to the requirement that the corresponding strains be zero on these surfaces. A refined displacement field is obtained by applying these boundary conditions in each region. It is important to note that several of the higher order terms in the generalized displacement field are either found to be zero or are defined in terms of the lower order functions. Additional boundary conditions must be imposed to ensure the continuity of displacements at the interface of the nondelaminated and the delaminated regions. This continuity conditions can be exactly satisfied with the classical theory since it assumes a linear displacement distribution through the thickness. However, the displacement distribution using the refined theory is nonlinear and therefore the continuity conditions can be satisfied in an average sense.

The finite element method (FEM) is used to implement the refined higher order theory since it allows for the analysis of practical geometries and boundary conditions. The continuity conditions are also easily implemented using FEM. The finite element equations are derived using the discretized form of Hamilton's principle, which is stated as follows

$$\delta\prod=\int_{t1}^{t2}\sum_{e=1}^{N_e}\left[\delta K^e-\delta U^e+\delta W^e\right]dt=0 \tag{5}$$

where t_1 and t_2 are the initial and the final times, respectively and δK^e, δU^e and δW^e are the element variations in the kinetic, strain and potential energies, respectively. The finite element matrices are formulated as follows.

$$\int_{t_1}^{t_2}\sum_{e=1}^{N_e}\left[\delta w^e\, M^e\,\ddot{w}^e+\delta w^e\, K^e\, w^e-\delta w^e\, F_p^e\right]=0 \tag{6}$$

where N_e is the number of elements, an overdot indicates a derivative with respect to time and the nodal degrees of freedom for each element are specified as follows.

$$\mathbf{w}_n^e=\left[u_n\ v_n\ w_n\ \frac{\partial w_n}{\partial x}\ \frac{\partial w_n}{\partial y}\ \phi_{xn}\ \phi_{yn}\right] \tag{7}$$

The linear finite element equations of motion are expressed as follows.

$$M\,\ddot{w}+K\,w=F_p \tag{8}$$

The quantities M, K , and w denote the mass and stiffness matrices, and the nodal displacement vector, respectively. The quantity F_p is the force vector due to piezoelectric actuation. A total of five segmented piezoelectric materials are used as control actuators. Bilinear shape functions are used for the inplane displacements and rotations (u, v, ϕ_x, ϕ_y) while a 12 term cubic polynomial is used for the transverse displacement (w). The resulting four noded rectangular elements are nonconforming for computational efficiency and contain 28 degrees of freedom each. Once the finite element model has been constructed, it is necessary to implement the continuity conditions to ensure continuity of displacements at the interface of the nondelaminated and delaminated regions. These conditions are enforced in the finite element implementation using a penalty approach. More details about this procedure can be found in Ref. [18].

2.2. Unsteady Aerodynamics and Rational Functions Approximation

After vibration analysis, a modal reduction is performed using the first six elastic modes. A doublet lattice method is used to compute the unsteady aerodynamic forces and the unsteady gust forces. Including the aerodynamic forces, the equations of motion for aeroservoelastic analysis can be written as

$$M_s\ddot{\xi} + C_s\dot{\xi} + K_s\xi = \overline{F}_p + Q_a\xi + Q_G\frac{w_G}{V} = \overline{F}_p + q_d(A_a\xi + A_G\frac{w_G}{V}) \tag{9}$$

where ξ represents the generalized modal coordinates, q_d is the dynamic pressure. The quantities M_s, C_s, and K_s are the generalized mass, the damping, and the stiffness matrices in modal coordinates. Matrices Q_a and Q_G are the generalized aerodynamic forces due to flexible modes and gust, respectively. The aerodynamic forces are approximated as the transfer functions of the Laplace variable using a least square curve fit approximation to define the aeroservoelastic equations of motion in a linear time invariant state-space form. Roger's method [19] approximates the unsteady aerodynamic forces in the following form.

$$A_{ap} = [A_\xi A_g] = \overline{P}_0 + \overline{P}_1 s' + \overline{P}_2 s'^2 + \sum_{j=3}^{N}\frac{\overline{P}_j s'}{s'+\gamma_{j-2}} \tag{10}$$

where $\overline{P} = [P_\xi P_g]$, $s' = ik = i\omega b/V = sb/V$ and s is the Laplace variable, the quantity k is the reduced frequency, b is the semi-chord and V is the airspeed. Subscripts ξ and g indicate elastic, control surface and gust modes, respectively and γ_{j-2} are the aerodynamic poles which are usually preselected in the range of reduced frequencies of interest. In this study, four terms of the aerodynamic poles are included for the rational functions approximation. The augmented aerodynamic state is defined as follows.

$$x_{ja} = \frac{s'}{s'+\gamma_{j-2}}[P_{j\xi}\, P_{jg}]\begin{Bmatrix}\xi\\ w_g\end{Bmatrix}, \quad j=3,4,5,6. \tag{11}$$

Using the rational function approximation, the system equations of motion is written in the following form.

$$\{\dot{x}_s\} = [A_s]\{x_s\} + [B_p]\{u\} + [B_G]\{w_G\} \tag{12}$$

where

$$\{x_s\} = \lfloor \xi^T \quad \dot{\xi}^T \quad x_a^T \rfloor^T \tag{13.a}$$

$$\{u\} = \lfloor V_1 \quad V_2 \quad V_3 \quad V_4 \quad V_5 \rfloor^T \tag{13.b}$$

$$\{w_G\} = \lfloor w_g \quad \dot{w}_g \rfloor^T \tag{13.c}$$

x_a denotes the augmented aerodynamic states, {u} is the control voltage vector.

The vertical gust is modeled using a second order Dryden model as follows [19]

$$\frac{w_g}{w} = \sigma_{wg}\frac{\sqrt{\frac{3V}{L}}\left(s+\frac{V}{L\sqrt{3}}\right)}{\left(s+\frac{V}{L}\right)^2} \tag{14}$$

where σ_{wg} is the RMS (root mean square) value of the gust velocity, L is the characteristic gust length and V is the airspeed. When the low pass filter is included, the state space equation of gust can be expressed as follows.

$$\{\dot{x}_g\} = [A_g]\{x_g\} + \{B_g\}w$$
$$\{w_G\} = [C_g]\{x_g\} \tag{15}$$

Including the gust dynamics system, the following state space equations are obtained.

$$\{\dot{x}\} = [A]\{x\} + [B]\{u\} + \{B_w\}w$$
$$\{y\} = [C]\{x\} \tag{16}$$

The resulting state space model is 39th order including six elastic modes, twenty four aerodynamic states, and three gust states.

3. AEROEASTIC CONTROL SYSTEM DESIGN FOR GLR

For a given design airspeed, a controller for GLR (gust load reduction) of the delaminated plate is designed. The following output feedback control law is introduced.

$$\{u\} = -[K_G]\{y\} \tag{17}$$

where $[K_G]$ denotes output feedback gain and $\{y\}$ includes only structural information. The eigenvalue problem of the closed-loop system can be written as

$$([A]-[B][K_G][C])\{\phi^c\}_i = -\lambda_i^c\{\phi^c\}_i \tag{18}$$

where $\{\phi^c\}_i$ is the eigenvector of the closed-loop system corresponding to the eigenvalue λ_i^c. The eigenvalues of the structural modes can be assigned to desired values by using a pole placement technique. It must be noted that all the eigenvalues of the closed-loop system are maintained in the stable region even though only the eigenvalues of the structural modes are assigned to desired locations. This is due to the fact that the aerodynamic and the gust modes are not influenced much by the output feedback control system.

The problem can be stated as a nonlinear parameter optimization problem where it is necessary to impose specified eigenspace equality constraints and the elements of output feedback gain matrix are the parameters to be determined. Defining $\{p\}$ as the parameter vector that consists of the elements of output feedback gain $[K_G]$, the nonlinear programming problem can be formulated as follows.

$$\begin{gathered}\text{Determine output feedback gain parameter } \{p\} \\ \text{subject to} \\ f_i(\{p\}) = \lambda_i^d - \lambda_i(\{p\}) = 0, \quad i = 1,2,...,Ns\end{gathered} \tag{19}$$

where $f_i(\{p\})$ represents the equality constraints associated with the closed-loop eigenvalue assignment, Ns is the number of structural modes and λ_i^d denotes the desired eigenvalues of these modes. The above problem can be solved by using any gradient-based nonlinear programming algorithm. In this study, homotopic nonlinear programming with minimum norm correction algorithm is used [20,21]. To enhance convergence, the linear homotopy map is generated. The original eigenvalue assignment problem is replaced by the one-parameter α family as follows.

$$f_i(\{p\}) = \alpha\lambda_i^d + (1-\alpha)\lambda_i(\{p_{start}\}) - \lambda_i(\{p\}) = 0, \quad 0 \le \alpha \le 1 \tag{20}$$

where $\{p_{start}\}$ is the initial starting value of the parameter vector. Sweeping α using a suitably small increment generates a sequence of neighboring problems. These sequences of problems are solved using the neighboring converged solutions to generate starting iterative for each subsequent problem. The desired solution is reached once solution for $\alpha = 1$ is obtained. The local design corrections for each α are performed by linearizing the neighboring problem (nonlinear constraint equations) about the local solution and by computing the minimum norm differential correction that satisfies the linearized constraint equation [22]. More details about this design algorithm can be found in Ref. [23].

After designing the control system and determining the gain matrix, the gust responses of the delaminated plate model are calculated. The square of the RMS of the system outputs (the modes of the system) is computed as follows.

$$\sigma_i^2 = \left[[C][X][C]^T\right]_{ii}, \quad i = 1,2,..,Ns \tag{21}$$

The state covariance matrix [X] of the closed-loop system is the solution of a Lyapunov equation in the following form [24]

$$[A_c][X] + [X][A_c]^T + \{B_w\}Q_w\{B_w\}^T = 0 \tag{22}$$

where Q_w is the intensity of white noise.

4. NUMERICAL EXAMPLE AND RESULTS

Simple smart composite plates with one edge clamped and others free are considered for the numerical example. The natural frequencies are investigated for plates with and without a small delamination (Fig. 2). The results are presented for a *[-45°/45°/0°]$_S$* Graphite/Epoxy laminate with five pairs of surface bonded actuators. Each composite layer has uniform thickness of *0.0000134m*. The length of the plate is *0.305m*, the width is *0.076m* and the total thickness is *0.000804m*. The five segmented piezoelectric materials are attached as shown in Fig.2. A delamination is also assumed to be placed at midplane in the region between $0.0305<x<0.061$ *m*, and $0.0152<y<0.0456$ *m*. The material properties are : $E_1=98.0$ *GPa*, $E_2=7.9$ *GPa*, $\nu_{12}=0.28$, $G_{12}=G_{13}=5.6$ *GPa*, $G_{23}=2.4$ *GPa*, $\rho=1520$ *Kg/m^3* for the composite plate and $E=63$ *GPa*, $\nu=0.31$, $G=24.2$ *GPa*, $\rho=5000$ *Kg/m^3*, $d_{12}=250\times10^{-12}$ *m/V* for the piezoelectric materials. Table 1 shows the effect of delamination on the natural frequencies of the composite plate. The first six natural frequencies of the composite plate with and without delamination are presented. Significant changes in the first three frequencies (28% change in 1st mode, 10% in 2nd mode and 5% in 3rd mode) are observed as a result of the small reduction in the structural stiffness due to delamination. However, changes in frequencies of the higher modes due to delamination are negligible.

The open loop flutter analysis is conducted for both delaminated and nondelaminated composite plates. Figures 3 and 4 show the changes in the eigenvalues of the open loop system for the nondelaminated and the delaminated plates, respectively. It is observed that the second mode of both models becomes unstable as airspeed increases. The flutter speed of the nondelaminated and the delaminated plate models are *26.2 m/sec (27.0 Hz)* and *25.2 m/sec (24.8 Hz)*, respectively. About five percent reductions in the flutter speed is observed due to the presence of delamination which can be very critical. Using the delaminated plate model, an active control system for GLR is designed at the design airspeed of *25.0 m/sec*, which is chosen arbitrarily. The pole placement technique that is described in the previous section is used for designing the control system. The GLR system is designed assuming that the six elastic modes are measurable. The preassigned eigenvalues of the closed loop system are λ_c= *-95.4 ± i 89.3, -10.3 ± i 160.3, -12.6 ± i 275.1, -15.1 ± i 530.4, -17.4 ± i 970.9, -9.6 ± i 1132.1.* Table 2 shows the eigenvalues of both open and closed loop systems at the design airspeed. Significant changes are observed in the real part of the eigenvalue corresponding to the second mode. This is due to the fact that a larger weight is imposed on the second mode since the second mode of the open loop system makes the system become unstable. Table 3 presents the RMS values of the elastic modes due to gust for the open loop system of the nondelaminated plate and the open and closed loop systems of the delaminated plate model. As shown in this table, the RMS values of the first three modes for the closed loop system of the delaminated plate model are reduced up to 78% compared to the open loop case. However, the RMS values of two higher modes for the closed loop system are increased. This increase is not expected to affect the performance of the GLR system, since the contribution of the higher modes to the system is much smaller compared to the contribution of the lower modes. Figure 5 shows the eigenvalue changes over the airspeed range for the closed loop system when the GLR

system is designed at the prescribed design velocity, *25.0 m/sec*. The figure indicates stability up to design speed and flutter occurs at about *27.1 m/sec*. Figure 6 presents the RMS values of the first three modes due to gust, over a range of airspeed, of the open loop system for the nondelaminated and delaminated plate models and the closed loop system for the delaminated plate model. It can be seen that active control system of the delaminated plate model yields good control performance for gust load reduction compared to the open loop case. For the closed loop system of the delaminated plate model, flutter occurs at about *27.1 m/sec*.

To investigate the control performance of the designed system, the time histories of the tip displacement and twist and the control voltages applied to the actuators are calculated. Figure 7 shows the time histories of the open loop and closed loop systems due to disturbances at the design airspeed for the nondelaminated and the delaminated plate models. As shown in this figure, the open loop system for the delaminated plate model exhibits a harmonic motion. That is due to the fact that the delaminated plate model becomes unstable at *25.2 m/sec*, which is very close to the design airspeed. Figure 7 also shows that the control system makes the delaminated plate model more stable than the nondelaminated plate model. Figure 8 shows the control voltage applied to the actuators due to the disturbance. It can be seen that maximum applied voltage is less than 80 Volts. This figure also shows that the applied voltages to the actuators (1, 2, 5) and (3, 4) are in the same phase. This combination of the control voltages can efficiently control the higher bending mode (second bending mode) which causes the model to flutter.

5. SUMMARY

The refined higher order theory for analyzing an adaptive composite plate in the presence of delaminations is used. The theory accurately captures the transverse shear deformation through the thickness. The effects of delamination on the aeroelastic characteristics of composite plates are investigated. And an active control system is designed to redistribute the loads and to minimize the effect of delamination. The following observations are made from this study.

(1) Significant changes in the first three frequencies are observed as a result of the small reduction in the structural stiffness due to delamination.

(2) From the example model, it is observed that there is about five percent reductions in the flutter speed due to the presence of delamination which can be very critical.

(3) The active control system of the delaminated plate model yields good control performance for gust load reduction compared to the open loop case. The RMS values for the closed loop system of the delaminated plate model are reduced up to 78% compared to the open loop case.

(4) The aeroelastic control results show that controller makes the delaminated plate model behave like a normal plate.

ACKNOWLEDGMENTS

The research was supported by the Air Force Office of Scientific Research, grant number: F49620-96-0195, technical monitor Dr. Brian Sanders.

REFERENCES

1. Lee, C. K. "Theory of Laminated Piezoelectric Plates for the Design of Distributed Sensors/Actuators. Part 1: Governing Equations and Reciprocal Relationships" *Journal of the Acoustical Society of America*, Vol. 87, No. 3, March, 1990. pp. 1144-1158.

2. Chandrashekhara, K. and Agarwal, A. N. "Active Vibration control of Laminated Composite Plates Using Piezoelectric Devices: A Finite Element Approach" *Journal of Intelligent Material Systems and Structures*, Vol. 4, Oct. 1993, pp. 496-508.

3. Chattopadhyay, A. and Seeley, C. E. "A Higher Order Theory for Modeling Composite Laminates with Induced Strain Actuators" *Composites Part B: Engineering*, Nov. 1997.

4. Yang, H. T. and He, C. C., "Three-Dimensional Finite Element Analysis of Free Edge Stresses and Delamination of Composite Laminates", *Journal of Composite Materials*, Vol. 28, No. 15, 1994, pp. 1394-1412.

5. Whitcomb, J. D., "Three Dimensional Analysis of a Postbuckled Embedded Delamination", *Journal of Composite Materials*, Vol. 23, 1989, pp. 862-889.

6. Pavier, M. J. and Clarke, M. P., "A Specialized Composite Plate Element for Problems of Delamination Buckling and Growth" *Composite Structures*, Vol. 35, 1996, 45-53.

7. Whitcomb, J. D., "Finite Element Analysis of Instability Related Delamination Growth" *Journal of Composite Materials*, Vol. 15, 1981, pp. 403-426, ,

8. Kardomateas, G. A and Schmueser, "Buckling and Postbuckling of Delaminated Composites Under Compressive Loads Including Transverse Shear Effects", *AIAA Journal*, Vol. 26, No. 3, 1988, pp. 337-343.

9. Gummadi, L. N. B. and Hanagud, S. (1995) "Vibration Characteristics of Beams with Multiple Delaminations" *Proc. 36th AIAA/ASME/ASCE/AHS/ASC Structures, Structural Dynamics and Materials Conference - Adaptive Structures Forum,* New Orleans, LA, Apr. 10-14, pp. 140-150.

10. Barbero, E. J. and Reddy, J. N., "Modeling of Delamination in Composite Laminates Using a Layer-wise Plate Theory" *International Journal of Solids and Structures*, Vol. 28, No. 3, 1991, pp. 373-388.

11. Chattopadhyay, A. and Gu, H. "A New Higher-Order Plate Theory in Modeling Delamination Buckling of Composite Laminates" *AIAA Journal*, Vol. 32, No. 8, 1994, Aug., pp. 1709-1718.

12. Chattopadhyay, A. and Gu, H. "Elasticity Solution for Delamination Buckling of Composite Plates", *Proc. 37th AIAA/ASME/ASCE/AHS/ASC Structures, Structural Dynamics and Materials Conference*, Salt Lake City, UT, Apr. 15-18. 1996.

13. Chattopadhyay, A. and Gu, H. "An Experimental Investigtion of Delamination Buckling and Postbuckling of Composite Laminates" *Proc. ASME International Mechanical Engineering Congress and Exposition*, Atlanta, GA, Nov. 17-22, 1996.

14. Chattopadhyay, A., Nam, C., Dragomir-Daescu, D., Gu, H., "Dynamics of Smart Composites including Delamination," *12th Eigineering Mechanics Conference*, La Jolla, CA, May 17-20, 1998.

15. Chattopadhyay, A., Dragomir-Daescu, D., and Nam, C., "Active Control of Delaminated Composite Plates with Piezoelectric Actuators and Sensors," *13th Annual Conference of the American Society of Composites (ASC),* Baltimore, September 1998.

16. Chattopadhyay, A., Dragomir-Daescu, D., and Nam, C., "An Investigation of Delaminated Smart Composite Plates for Damage Detection," *The 1998 International mechanical Engineering Congress & Exposition,* Anaheim, November 1998.

17. Seeley, C. E. and Chattopadhyay, A. "Modeling Delaminations in Smart Composite Laminates" *Proc. of the 37th AIAA/ASME/ASCE/AHS/ASC Structures, Structural Dynamics and Materials Conference and Adaptive Structures Forum*, Salt Lake City, UT, Apr. 15-19, 1996, pp. 109-119.

18. Chattopadhyay, A., Charles, S.E. "Modeling of Smart Composite Laminates Including Debonding: A Finite Element Approach," *38th Structures, Structural Dynamics and Materials Conference and Adaptive Structures Forum*, Kissimmee, FL, April 1997.

19. Tiffany, S.H., Adams, W.M., "Nonlinear Programming Extensions to Rational Function Approximation Methods for Unsteady Aerodynamic Forces," NASA-TP-2776, 1998.

20. Junkins, J.L., and Kim, Y., *Introduction to Dynamics and Control of Flexible Structures*, AIAA, Washington, DC, 1993.

21. Dunyak, J.P., Junkins, J.L., and Watson, L.T., "Robust Nonlinear Least Square Estimation Using the Chow-Yorke Homotopy Method," *Journal of Guidance, Control, and Dynamics*, Vol.7, No.6, 1984, pp.752-755.

22. Junkins, J.L., "Equivalence of the Minimum Norm and Gradient Projection Constrained Optimization Techniques," *AIAA Journal,* Vol.10, No.7, 1972, pp.927-929.

23. Nam, C., Chattopadhyay, A., Kim, Y., "An Optimal Wing Planform Design for Aeroelastic Control," *7th AIAA/USAF/NASA/ISSMO Symposium on Multidisciplianry Analysis and Optimization*, St. Louis, MI, Sept. 2-4, 1998, submitted to the *AIAA Journal.*

24. Livne, E., Schmit, L.A., and Friedmann, P.P., "Towards Integrated Multidisciplinary Synthesis of Actively Controlled Fiber Composite Wings," *Journal of Aircraft*, Vol.27, No.12, 1990, pp.979-992.

Table 1. Natural frequencies of the nondelaminated and delaminated plates.

Mode No.	Nondelaminated Plate (Hz)	Delaminated Plate (Hz)
1	5.84E+00	4.20E+00
2	3.28E+01	2.95E+01
3	5.88E+01	5.64E+01
4	8.98E+01	8.71E+01
5	1.66E+02	1.59E+02
6	1.87E+02	1.84E+02

Table 2. Eigenvalues of the open loop and closed systems for delaminated plate model at design airspeed.

Open Loop Real ± I Imaginary(Hz)	Closed Loop Real ± I Imaginary(Hz)
-1.07E+01 ± I 1.80E+02	-9.66E+00 ± I 1.80E+02
-1.85E+01 ± I 1.54E+02	-1.74E+01 ± I 1.55E+02
-1.61E+01 ± I 8.45E+01	-1.51E+01 ± I 8.45E+01
-1.07E+01 ± I 4.34E+01	-1.27E+01 ± I 4.38E+01
-3.75E-01 ± I 2.48E+01	-1.04E+01 ± I 2.55E+01
-1.03E+02 ± I 1.38E+01	-9.55E+01 ± I 1.42E+01
-2.77E+02 ± I 1.82E+01	-2.78E+02 ± I 1.82E+01
-6.18E+02 ± I 0.00E+00	-6.25E+02 ± I 0.00E+00
-5.84E+01 ± I 0.00E+00	-5.62E+01 ± I 0.00E+00
-5.67E+02 ± I 0.00E+00	-5.63E+02 ± I 0.00E+00
-5.22E+02 ± I 1.50E+00	-5.21E+02 ± I 1.52E+00
-5.26E+02 ± I 2.65E-01	-5.26E+02 ± I 2.65E-01
-3.51E+02 ± I 0.00E+00	-3.57E+02 ± I 0.00E+00
-3.98E+02 ± I 1.17E+00	-3.98E+02 ± I 1.21E+00
-3.95E+02 ± I 1.37E-01	-3.95E+02 ± I 1.36E-01
-2.84E+02 ± I 0.00E+00	-2.79E+02 ± I 0.00E+00
-2.58E+02 ± I 0.00E+00	-2.59E+02 ± I 0.00E+00
-2.64E+02 ± I 0.00E+00	-2.65E+02 ± I 0.00E+00
-2.63E+02 ± I 4.34E-02	-2.63E+02 ± I 4.50E-02
-1.31E+02 ± I 0.00E+00	-1.31E+02 ± I 0.00E+00
-1.32E+02 ± I 0.00E+00	-1.32E+02 ± I 0.00E+00
-1.31E+02 ± I 0.00E+00	-1.31E+02 ± I 0.00E+00
-1.32E+02 ± I 0.00E+00	-1.32E+02 ± I 0.00E+00
-1.32E+02 ± I 0.00E+00	-1.32E+02 ± I 0.00E+00
-1.25E+00 ± I 0.00E+00	-1.25E+00 ± I 0.00E+00
-1.25E+00 ± I 0.00E+00	-1.25E+00 ± I 0.00E+00
-5.00E+02 ± I 0.00E+00	-5.00E+02 ± I 0.00E+00

Table 3. RMS values due to gust at design airspeed of V=25 m/sec for the nondelaminated and delaminated plate.

	Nondelaminated Plate(Open Loop)	Delaminated Plate(Open Loop)	Delaminated Plate(Closed Loop)
Mode 1	9.94E-01	3.23E+00	1.04E+00
Mode 2	6.17E-01	2.80E+00	6.20E-01
Mode 3	1.74E-01	6.45E-01	1.94E-01
Mode 4	2.25E-02	3.60E-02	2.78E-02
Mode 5	7.53E-03	1.80E-02	1.85E-02
Mode 6	4.92E-03	4.77E-03	5.86E-02

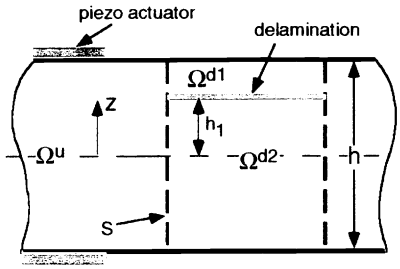

Fig. 1 Laminate cross section.

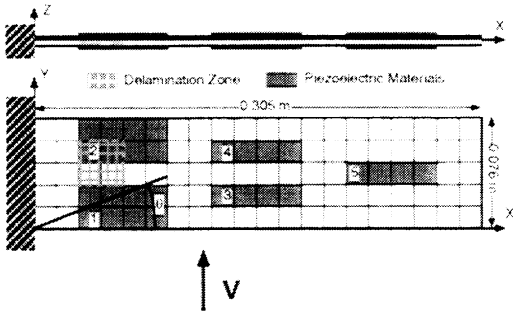

Fig. 2 Delaminated plate model with piezoelectric actuators.

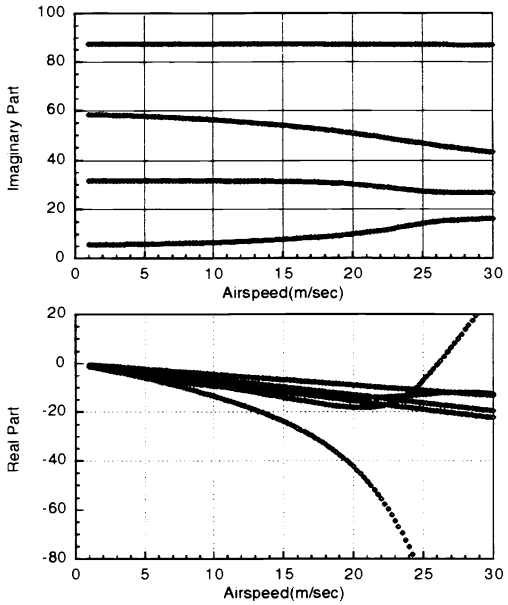

Fig. 3 Locus of eigenvalues of the open loop system for nondelaminated plate

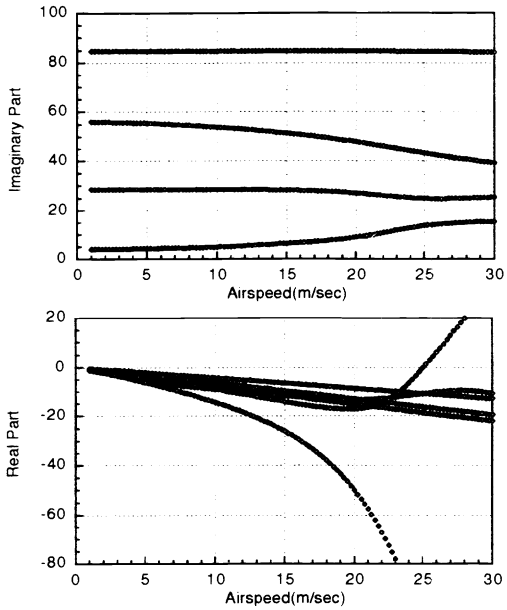

Fig. 4 Locus of eigenvalues of the open loop system for delaminated plate

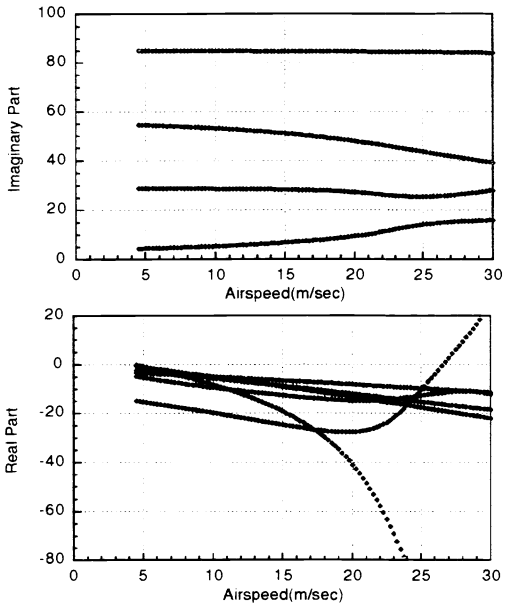

Fig. 5 Locus of eigenvalues of the closed loop system for nondelaminated plate

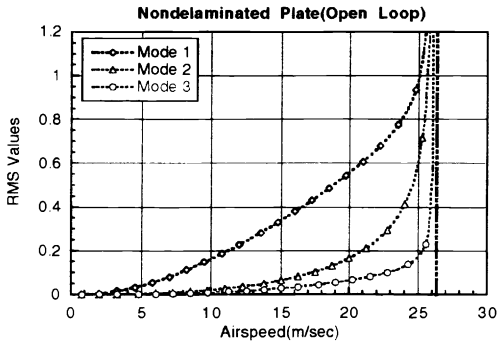

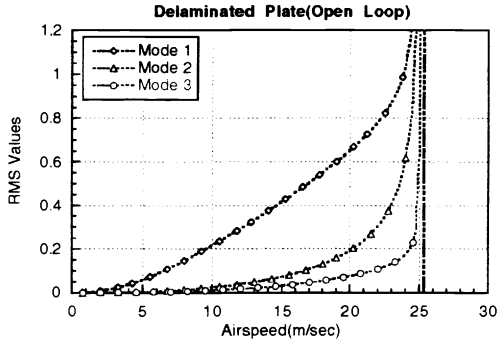

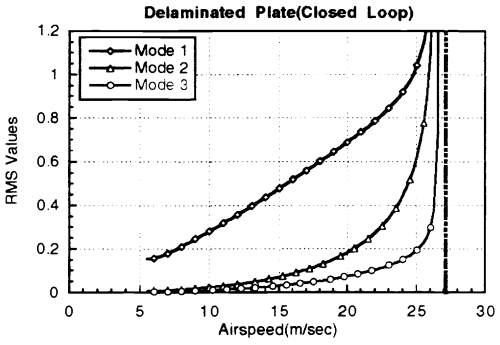

Fig. 6 RMS values of the elastic modes;
(a) Open loop of nondelaminated plate,
(b) Open loop of delaminated plate,
(c) Closed loop of delaminated plate.

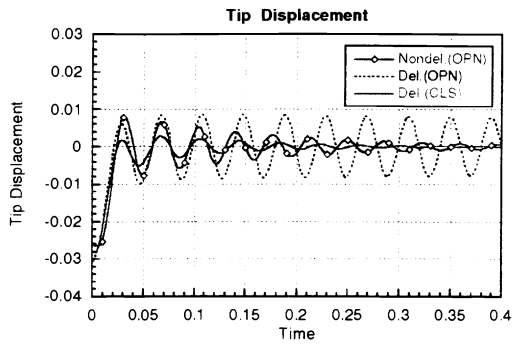

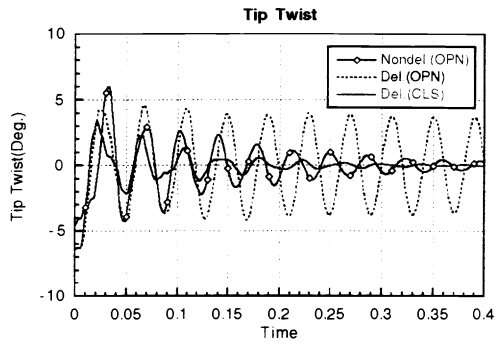

Fig. 7 Closed loop time responses at the design airspeed, 25m/sec; (a)Tip displacement, (b)Tip twist.

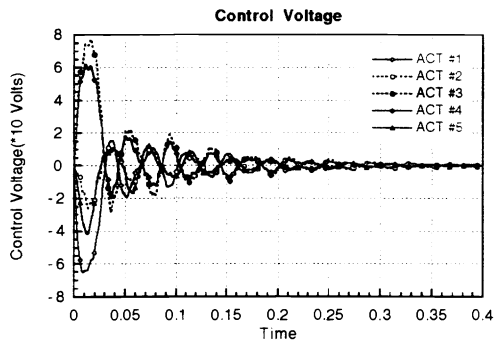

Fig. 8 Control voltages applied to the actuators.